Using the overall variation trend and fitting of Na-feldspar crystal plane spacing after chemical corrosion to prevent rock disasters

Zhengliao Zhang, Jinchun Xue*, Yunshuai Wan

School of Energy and Mechanical Engineering, Jiangxi University of Science and Technology, Nanchang 330013, Jiangxi, China

Abstract. Sulfuric acid pollution, caused by acid rain, acidic wastewater, and natural acidic wastewater from mines, poses a significant risk to the stability of natural stone slopes and human stone structures. This study aims to develop a non-mechanical testing method for assessing the degree of acid corrosion in rocks, facilitating early intervention by safety engineers. The proposed method involves using XRD to measure the crystal plane spacing of Na-feldspar corroded by different concentrations of sulfuric acid, followed by mathematical analysis to determine the overall deviation degree of the crystal plane spacing. Four Deviation indices were defined to characterize the degree of acid corrosion, and all four indices increased with increasing acidity. By comparing trend charts, an optimized number of crystal planes for analysis was identified. Selecting the 100 sets of data with the largest spacing yielded similar trend results as selecting all the data. In addition, five different fitting methods were compared, and the power function fitting of Weighted Sum of squares of cumulative errors (WSSCE) was found to provide the optimal empirical formula, with a correlation coefficient exceeding 0.98.

1 Introduction

On the one hand, with many mines being exploited by humans, the stone slopes of some mines containing natural acidic wastewater are being corroded and damaged. On the other hand, due to high human sulfur dioxide emissions, acid rain is causing increasingly severe damage to open-air stone buildings, roads, sculptures, bridges, foundation piles, and other structures. In addition, some acidic waste liquids caused by industrial production also cause pollution. The chemical corrosion damage of rocks caused by acidic pollution is threatening the sustainability of various natural and artificial stone structures. Once the damage to rocks reaches a critical point, hard rock disasters will occur. For safety engineers, to prevent and control rock disasters, it is necessary to promptly understand the degree of rock corrosion. The most widely used testing method currently is mechanical testing, which uses the decrease in rock mechanical strength to characterize the degree of rock corrosion [1,2,3,4,5,6]. However, mechanical testing methods have some unfavorable factors or limitations, such as: (1) In order to meet the requirements of the International Society of Rock Mechanics [7,8,9], mechanical testing methods usually require pre-treatment such as sample preparation, cutting, grinding, polishing, etc. These pre-treatments require specialized equipment and a long process; (2) Static mechanical tests require a longer loading time, while dynamic impact tests require a specialized SHPB device, which is usually only available in very few mines; (3) Mechanical testing often requires a large number of samples to cover multiple points within the mining area that need to be tested, which can lead to difficulty in carrying samples; (4) In order to ensure the parallelism of the end face, it is easy to directly grind the outermost layer (i.e. the most severely corroded part) of the rock during the sample preparation process, resulting in the final mechanical test results not accurately reflecting the degree of rock corrosion. Therefore, it is necessary to find a characterization method that is more portable and can reflect the degree of surface corrosion of the sample.

Scanning experiments on rock powder using an XRD device can obtain crystallographic data of the rock. At present, these crystallographic data have been used to analyze many types of damage in rocks, such as thermal damage [10], high-humidity damage [11], freeze-thaw damage [12], wet-dry cycles damage [13], etc. However, these applications usually only use these crystallographic data for material composition retrieval, crystallinity calculation, and residual stress calculation. Even if it involves crystal plane spacing calculation, it does not involve the trend of omnidirectional crystal plane changes, this study will attempt to find and optimize crystallographic methods that can characterize macroscopic chemical corrosion damage in rocks from this perspective.

Na-feldspar is the main component of various rocks and widely exists in various stone structures. Since silica usually does not react chemically with sulfuric acid, while Na-feldspar can react chemically with sulfuric acid, it can be considered that Na-feldspar is the most important rock component destroyed by sulfuric acid. [14,15,16,17,18]. Therefore, this study attempted to conduct deviation index statistics on the crystal plane spacing data of Na-feldspar

*Corresponding author's email: xuejinchun@jxust.edu.cn

after chemical corrosion treatment, and finally successfully found a new method that can quickly identify the degree of rock corrosion.

2 Materials and Methods

The test sample is analytical pure grade Na-feldspar powder. The soaking experiment method involves treating Na-feldspar powder with sulfuric acid at pH 3.0, 2.0, 1.0, 0.5, and pure water at pH 7.0, and then waiting for 24 hours for natural air drying. These groups treated with sulfuric acid or water are defined as the treatment group (TR), while the untreated original Na-feldspar is defined as the control group (CK). Then, use an XRD device with the model of Malvern Panalytical Empyrean to scan the Na-feldspar powder that has undergone different treatments at 5 ~ 90°.

3 Results

3.1 Results of XRD

The XRD test results are shown in Fig.1. The method of calculating crystal plane spacing based on raw data obtained from XRD testing is commonly referred to as "Rietveld". This method has been integrated with various XRD software and is very convenient to use. In this study, MDI Jade 6 was chosen as the data processing software. [19,20,21]. The software was able to calculate about 1000 sets of crystal planes within the test range, sorted by distance from largest to smallest.

Since the results obtained from the XRD test are diffraction plane indices, the results include high-order diffraction planes (e.g. h k l not mutually prime) [22]. Although strictly speaking, high-order diffraction planes are different from primary crystal planes parallel to their direction (e.g. h k l mutually prime), the proportion of high-order diffraction planes in the 1000 sets of crystal planes is only 17.2%, and they are mostly concentrated in the latter half of the sorted results (e.g. crystal plane spacing is very small), with little impact on the overall results. Therefore, this study excluded the high-order diffraction plane part.

The remaining 828 sets of crystal planes were numbered sequentially from largest to smallest, respectively named Data No.1 to Data No. 828. Figure 2 shows the visualization results of the first 20 sets (e.g. Data No.1 ~ 20).

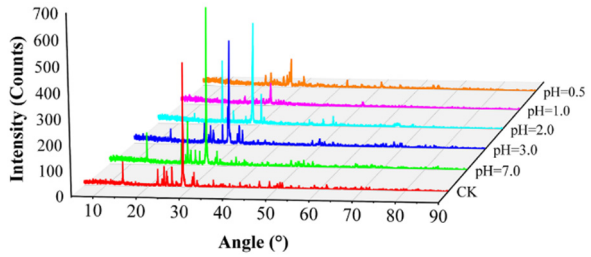

Fig. 1. Results of XRD.

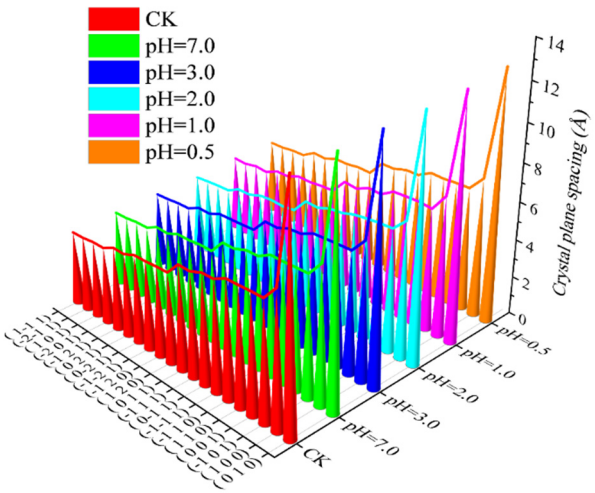

Fig. 2. Crystal plane spacing of Data No.1 ~ 20.

3.2 Results of Deviation index

Visually, in Figure 2, the variation amplitude of a single crystal plane is very small, and the change trend cannot be directly observed. Therefore, this study set up four different Deviation indices to measure the overall deviation of the TR group relative to the CK group. They are the Sum of squares of cumulative errors (SSCE), Weighted Sum of squares of cumulative errors (WSSCE), Weighted disorder degree (WDD), and the Sum of absolute values of differences (SAVD). The calculation methods are as follows:

$$SSCE = \Sigma [(d_i^{TR} - d_i^{CK})^2] \quad (1)$$

$$WSSCE = \Sigma [(d_i^{TR} / d_1^{CK}) \cdot (d_i^{TR} - d_i^{CK})^2] \quad (2)$$

$$WDD = \Sigma \{[(d_i^{TR} \cdot \left| d_i^{TR} - d_i^{CK} \right|) / (d_i^{CK})^2] / A\} \quad (3)$$

$$SAVD = \Sigma \left| d_i^{TR} - d_i^{CK} \right| \quad (4)$$

Among them, i, A, d_i^{TR}, d_i^{CK} and d_1^{CK} are Data No., the maximum number of selected data, the crystal plane spacing of Data No. i of TR, the crystal plane spacing of Data No. i of CK, and Data No.1 of CK. All summations are from Data No. 1 to Data No. A.

When software automatically processes data, it is possible to encounter a small amount of missing data in the TR group compared to the CK group, and the Data No. of these missing data is mostly in the latter part. This may be related to the fact that these crystal planes are too small to be submerged in noise, and these crystal planes are ignored at this time. In fact, Section 4.2 of this study demonstrates that the impact of these data with lower ranking on the overall calculation results is minimal and can be ignored.

When calculating SSCE, WSSCE, WDD and SAVD, as the data number increases, the value decreases and has a smaller overall impact. Therefore, this study divided the data into different subsets: 1 ~ 10, 1 ~ 20, 1 ~ 50, 1 ~ 100, 1 ~ 200, 1 ~ 300, 1 ~ 500, 1 ~ 800, and 1 ~ 828. These subsets were used to calculate the deviation levels separately. To demonstrate the rate of increase trend of the deviation index of crystal plane spacing under pH changes, the rates of increase of SSCE, WSSCE, WDD, and SAVD were calculated at pH=3.0, 2.0, 1.0, and 0.5 compared to pH=7.0. The rate of increase is represented by SSCE*, WSSCE*, WDD* and SAVD*. These were

done to prepare for optimizing the selection of data in the future. The results are shown in Table 1 (Due to the large amount of data, Table 1 only lists SSCE, WSSCE, WDD, and SAVD for Data No.1 ~ 100. For all 9 data subsets of SSCE, WSSCE, WDD, SAVD, SSCE*, WSSCE*, WDD*, and SAVD*, the visualization results are presented in Fig.5, Fig.6, Fig.7, and Fig.8 in Section 4.2).

Table 1. Results of deviation index.

Data No.	pH	Deviation index of crystal plane spacing			
		SSCE (Å²)	WSSCE (Å²)	SAVD (Å)	WDD (‰)
1 ~ 100	7.0	0.01105	0.00393	0.8133	2.45628
	3.0	0.01904	0.00667	1.1329	3.37902
	2.0	0.06370	0.02228	1.9451	5.82255
	1.0	0.09831	0.03446	2.2686	6.91054
	0.5	0.12245	0.06414	2.4618	7.33484

4 Analysis and Optimization

4.1 Overall analysis

Taking WSSCE as an example, Fig.3 and Fig.4 visually present the results of data in Table 1 through heat maps. Similar results can also be obtained for SSCE, WDD, and SAVD. In general, the deviation index increases with the enhancement of acidity, which demonstrates the effectiveness of the new method discovered in this study. The corresponding rate of increase changes exhibit good monotonicity and are suitable for fitting. By omitting the data with later numbers, similar results can still be obtained compared to selecting all the data, which demonstrates the potential for optimizing the amount of data selection for efficient calculation in practical engineering.

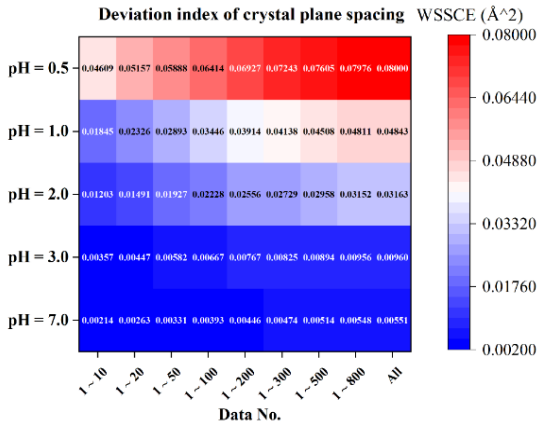

Fig. 3. Heat maps of WSSCE.

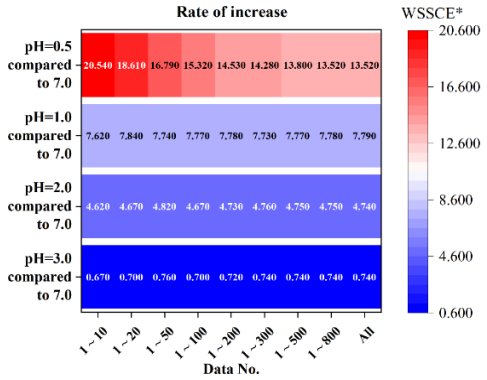

Fig. 4. Heat maps of WSSCE*.

4.2 Simplification of Deviation index

To optimize the amount of data selection, it is necessary to compare the consistency between the trend charts when selecting a small amount of data and when selecting all the data. Fig.5, Fig.6, Fig.7 and Fig.8 respectively show the trend charts of SSCE, SSCE*, WSSCE, WSSCE*, SAVD, SAVD*, WDD, and WDD*. To enhance the intuitiveness and rationality of the comparison process, the vertical axis of the dimensional indicators SSCE, WSSCE, and SAVD is adjusted so that the points coincide with the bottom frame when pH=7.0 and coincide with the top frame when pH=0.5, allowing them to vary with the change in data volume. The vertical axis of the dimensionless indicators SSCE*, WSSCE*, SAVD*, WDD, and WDD* is set at a constant value, ensuring that they do not change with the variation in data volume.

From the results of the line graph, when the data volume reaches 100, SSCE, SSCE*, WSSCE, WSSCE*, SAVD, SAVD*, WDD, and WDD* can all obtain highly consistent lines when selecting all data. Therefore, the selection of data volume can be optimized to the top 100 groups of data.

Certainly, selecting a data volume of less than 100 may also yield similar results, but to ensure monotonicity, the data volume should not be less than 20, as can be clearly seen from Fig.8 that when the data volume is too small, the trend of the WDD and WDD* graphs has changed significantly compared to when selecting all the data. This study suggests selecting no less than 100 data points to ensure that the optimized results remain highly consistent with those before optimization.

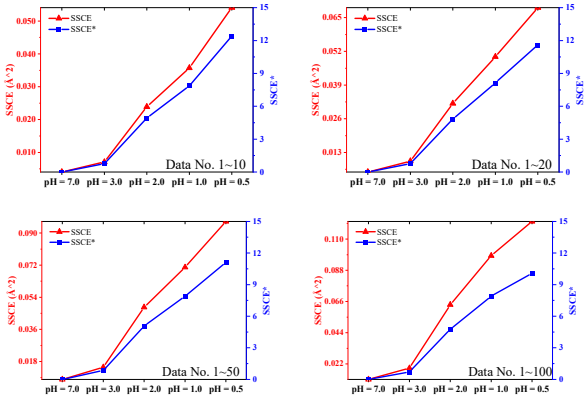

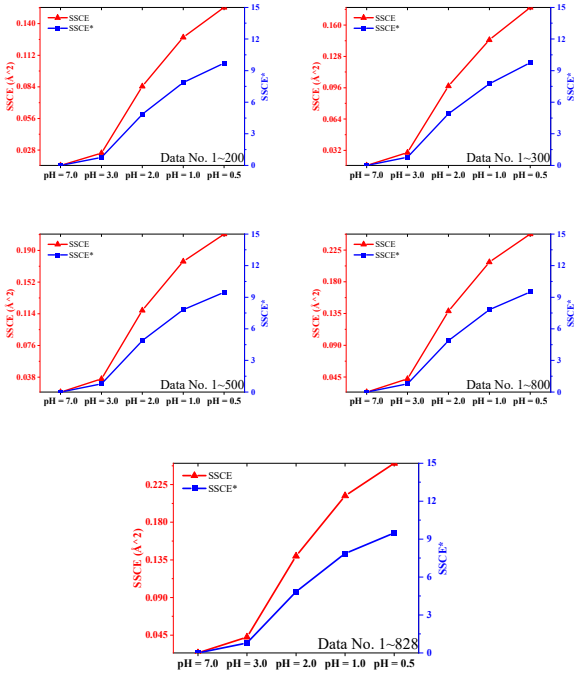

Fig. 5. Trend of SSCE and SSCE*.

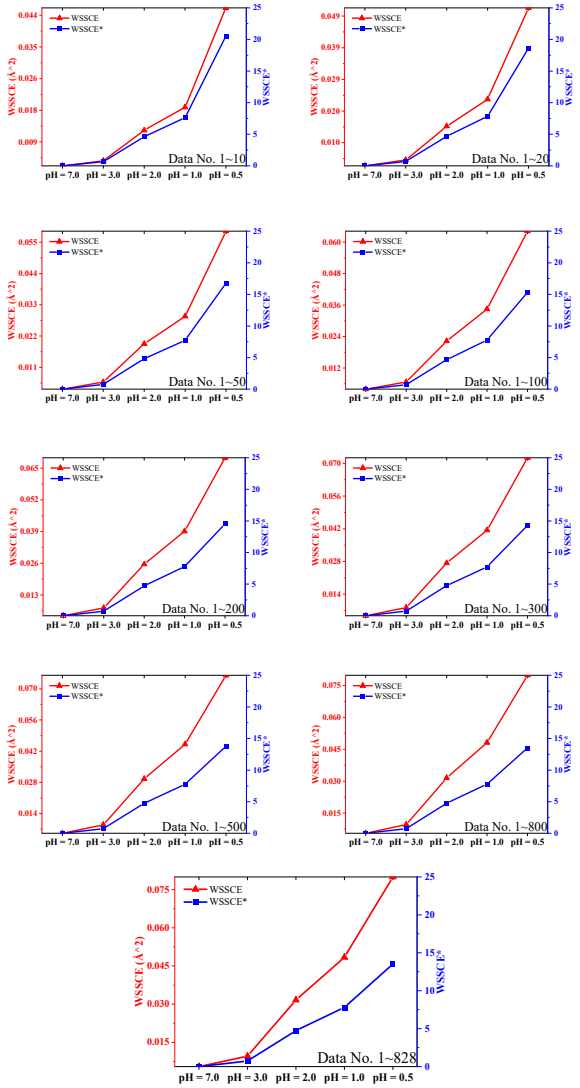

Fig. 6. Trend of WSSCE and WSSCE*.

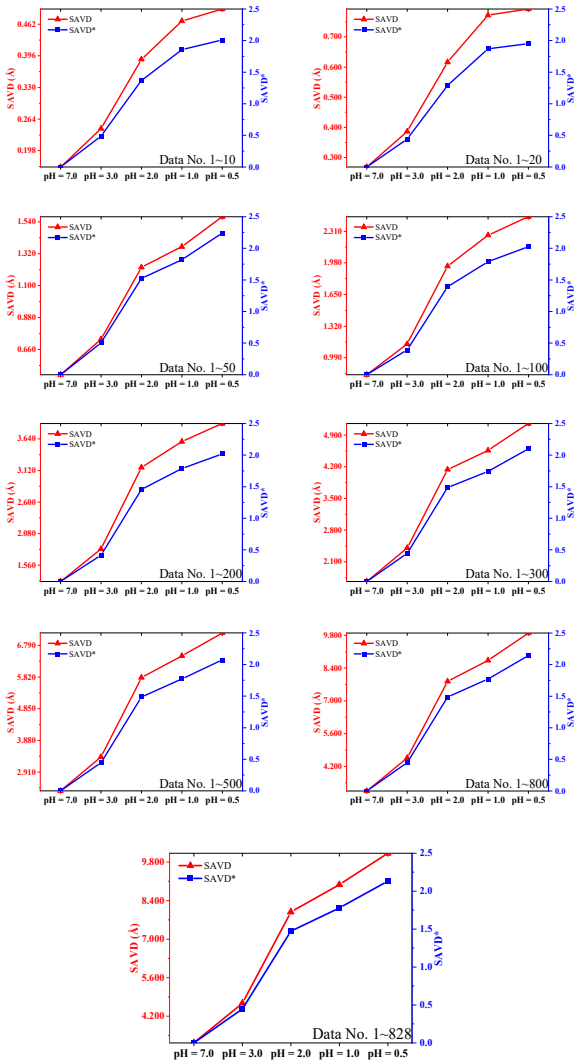

Fig. 7. Trend of SAVD and SAVD*.

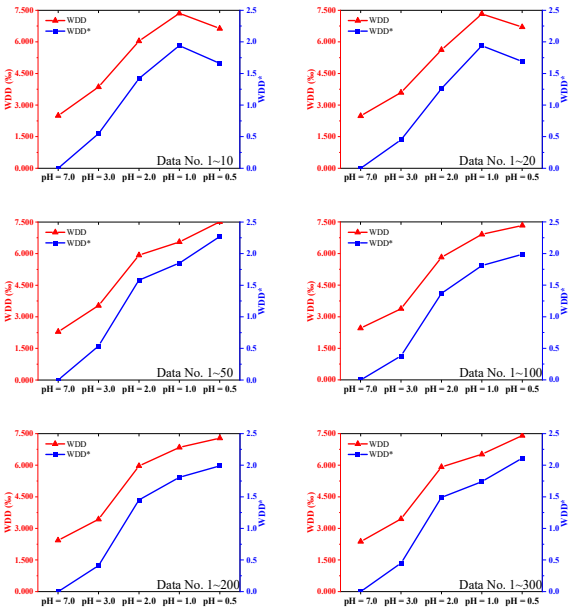

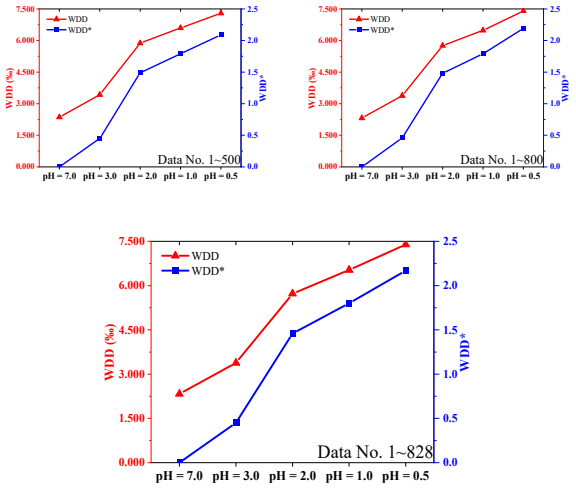

Fig. 8. Trend of WDD and WDD*.

4.3 Best index and fitting method

To select the most suitable deviation index from four types and determine the best fitting method, logarithmic function, power function, inverse proportion function, exponential function, and linear fitting were performed on Data No.1 to 100 for each deviation index. The deciding coefficient (e.g. the square of the correlation coefficient, R^2) of the fitting results were compared, and the visualized results are shown in Fig.9.

From Fig.9, all 20 fitting results from the four deviation indices and five fitting methods have correlations, and the linear fitting results are poor. The logarithmic function, power function, and exponential function fitting results have good deciding coefficients, all exceeding 0.92. Among the four deviation indices, WSSCE has the best fitting effect, with deciding coefficients exceeding 0.97 except for linear fitting. Among the 20 fitting results, the power function fitting of WSSCE has the best effect, with a deciding coefficient of 0.98238. Therefore, the power function fitting of WSSCE is selected as the best index and fitting method in this study. The fitted empirical formula is shown in Fig.10. The inverse formula of formula in Fig.10 is $pH = (20.95557 \cdot WSSCE + 0.07146)^{-0.9785} - 0.21375$.

In fact, as can be seen from Fig.5, Fig.6, Fig.7 and Fig.8, only the second derivative of the WSSCE curve is greater than 0, which serves as the deviation index in this study. This is favorable because pH is a logarithmic function and as pH linearly decreases, acidity increases exponentially. Therefore, the deviation index should ideally exhibit a larger variation when pH linearly decreases (e.g. second derivative greater than 0).

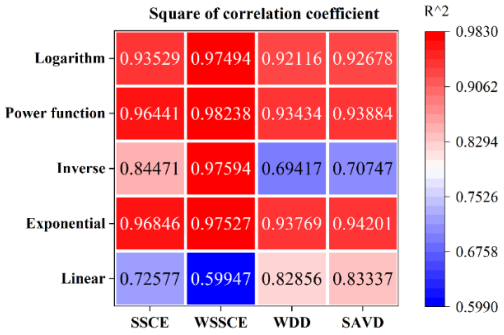

Fig. 9. Deciding coefficient of different fitting methods.

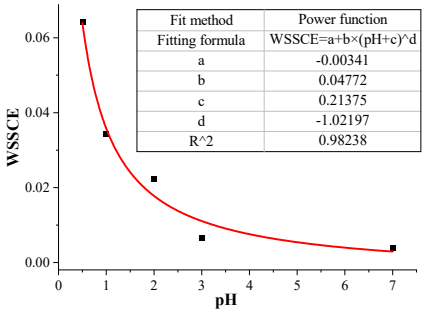

Fig. 10. Power function fitting of WSSCE.

5 Discussion

In addition to compensating for the shortcomings of mechanical experiments in the Introduction section, the new method discovered in this study also has some advantages compared to mechanical experiments: (1) the experimental instrument is an XRD device. Due to the simple operation and wide use of the XRD device, in addition to the purpose of this study, the XRD device can also play a huge role in mining and beneficiation fields [23,24,25,26]. However, mechanical testing equipment can usually only be used for mechanical testing. Therefore, when enterprises that need to pay attention to rock chemical corrosion damage have limited funds, it is more cost-effective to prioritize the purchase of XRD devices. When these enterprises only have XRD devices, this method will play a very important role. (2) Capable of supporting in-situ testing (e.g. testing at the same point at different times). Due to the limited number of powdered samples required for XRD testing (usually at the milligram level), it is possible to sample at the same location for a long time to observe the accumulation of chemical corrosion of Na-feldspar at that location over a certain period of time. The cutting machine or drilling machine used in mechanical testing during sampling will directly damage the same point when sampling multiple times.

6 Conclusion

To prevent hard rock disasters caused by chemical corrosion and sustainability of protecting stone structures, this study first conducted XRD experiments on acid-corroded Na-feldspar, then calculated the crystal plane

spacing using software. Subsequently, four different deviation indices, namely SSCE, WSSCE, WDD, and SAVD, were set to investigate the overall deviation of crystal plane spacing compared to the control group. The following conclusions were drawn:

(1) As acidity increased, SSCE, WSSCE, WDD, and SAVD all increased. Therefore, using the overall deviation of crystal plane spacing after acid corrosion of Na-feldspar as a measure of the degree of acid corrosion damage in rocks is effective.

(2) When a small amount of data was selected, the graph shapes (e.g. variation trends) of SSCE, WSSCE, WDD, and SAVD remained highly consistent with the selection of all data. This indicates that data volume can be optimized to make calculations more convenient in practical engineering applications. After comparison, the first 100 data points in descending order of crystal plane spacing were found to be sufficient, and the remaining data points can be omitted.

(3) By calculating the deciding coefficient of five different fitting methods, it was found that the 20 results obtained from the four deviation indices all indicated a correlation between pH and deviation index. Among them, the power function fitting of WSSCE showed the best fit, with a deciding coefficient of 0.98238.

In conclusion, by selecting the top 100 data points with the largest crystal plane spacing, WSSCE can be calculated first, and then the fitting formula $pH = (20.95557 \cdot WSSCE + 0.07146)^{-0.9785} - 0.21375$ can be used to indirectly assess the degree of acid damage in rocks. Certainly, in practical engineering, in-situ testing can also be directly performed to determine the chemical corrosion damage accumulated at a particular location during a specific period by calculating the increase in WSSCE. So that safety engineers can make timely arrangements to extend the life cycle of stone structures.

Acknowledgments

This study was funded by Graduate Innovative Special Fund Projects of Jiangxi Province (YC2022-S696).

References

1. Chen, Y.; Tong, H.; Chen, Q.; Du X.; Wang, S.; Pan, Y.; Dong, Y.; Ma, H. (2023) Chemical Corrosion-Water-Confining Pressure Coupling Damage Constitutive Model of Rock Based on the SMP Strength Criterion. Materials, 16, 6234. http://doi.org/10.3390/ma16186234
2. Chen, Q.; Chen, Y.; Xiao, P.; Du, X.; Pan, Y.; Azzam, R. (2023) Mechanical properties and damage constitutive model of sandstone after acid corrosion and high temperature treatments. International Journal of Mining Science and Technology, 33, 747-760. http://doi.org/10.1016/j.ijmst.2022.11.011
3. Liu, Y.; Liu, W.; Wang, C. (2023) Mechanical properties and constitutive model of fractured red sandstone under acid corrosion. SN Applied Sciences, 5, 1-13. http://doi.org/10.1007/s42452-023-05415-7
4. Xie, S.; Wan, W. (2020) Mechanical Damage to the Diorite Caused by Acid Corrosion. Geotechnical and Geological Engineering, 38, 3087-3094. http://doi.org/10.1007/s10706-020-01209-5
5. Zhao, Z.; Xue, J.; Jin, J.; Tan, L.; Cai, R.; Xia, W. (2022) Damage Analysis of Chemically Corroded Sandstone Under Cyclic Impacts and Axial Static Pressure. Geotechnical and Geological Engineering, 40, 2581-2592. http://doi.org/10.1007/s10706-022-02047-3
6. Xue, J.; Zhao, Z.; Dong, L. Jin, J.; Zhang, Y.; Tan, L.; Cai, R.; Zhang, Y. (2022) Effect of Chemical Corrosion and Axial Compression on the Dynamic Strength Degradation Characteristics of White Sandstone under Cyclic Impact. Minerals, 12, 429. http://doi.org/10.3390/min12040429
7. Bieniawski, Z.T.; Bernede, M.J. (1979) Suggested methods for determining the uniaxial compressive strength and deformability of rock materials: Part 1. Suggested method for determining deformability of rock materials in uniaxial compression. International Journal of Rock Mechanics and Mining Sciences & Geomechanics Abstracts, 16, 138-140. http://doi.org/10.1016/0148-9062(79)91451-7
8. Bieniawski, Z.T.; Bernede, M.J. (1979) Suggested methods for determining the uniaxial compressive strength and deformability of rock materials: Part 1. Suggested method for determination of the uniaxial compressive strength of rock materials. International Journal of Rock Mechanics and Mining Sciences & Geomechanics Abstracts, 16, 137. http://doi.org/10.1016/0148-9062(79)91450-5
9. Bieniawski, Z.T.; Hawkes, I. (1978) Suggested methods for determining tensile strength of rock materials - 1. suggested method for determining direct tensile strength. International Journal of Rock Mechanics and Mining Sciences, 15, 99-103. http://doi.org/10.1016/0148-9062(78)90003-7
10. Sunnetci, M.O.; Ersoy, H. (2022) A new perspective based on overcoming sample heterogeneity for the estimation of thermal damage inflicted on volcanic rocks using non-destructive tests. Rock Mechanics and Rock Engineering, 56, 1-22. http://doi.org/10.1007/s00603-022-03065-6
11. Chen, W.; Wan, W.; Zhao, Y.; He, H.; Wu, Q.; Zhou, Y.; Xie, S. (2022) Mechanical damage evolution and mechanism of sandstone with prefabricated parallel double fissures under high-humidity condition. Bulletin of Engineering Geology & the Environment, 81, 1-15. http://doi.org/10.1007/s10064-022-02747-3
12. Cui, K.; Liu, G.; Wu, G.; Zhu, P. (2019) Study on the characteristics and mechanisms of freeze-thaw damage of rock carrier of Helankou rock paintings under different conditions. Chinese Journal of Rock Mechanics and Engineering, 38, 1797-1808. http://doi.org/10.13722/j.cnki.jrme.2019.0054

13. Huang, Z.; Zhang, W.; Zhang, H.; Zhang, J.; Hu, Z. (2022) Damage characteristics and new constitutive model of sandstone under wet-dry cycles. Journal of Mountain Science, 19, 2111-2125. http://doi.org/10.1007/s11629-021-7239-8
14. Borges, R.M.K.; Amorim, L.E.D.; Rios, F.J.; Dos-Santos, G.C.S.; Freitas, M.E.; De-Lima, T.A.F.; Santos, A.; Pedrosa, T.A. (2022) Melt-melt immiscibility and implications for the origin of Madeira albite-rich granite, Pitinga mine, Amazonas, Brazil: A melt inclusion study. Brazilian Journal of Geology, 51. http://doi.org/10.1590/2317-4889202120210011
15. Koca T.K. (2023) The Effect of Geometrical Features of Release Surfaces on the Stability of Tectonically Disturbed Deep Rock Slopes in an Albite Open Pit Mine. Sustainability, 15, 1425. http://doi.org/10.3390/su15021425
16. Wang, P.; Tan, K.; Li, Y.; Xiao, W.; Liu, Z.; Tan, W.; Xu, Y. (2023) The adsorption of U(VI) by albite during acid in-situ leaching mining of uranium. Journal of Radioanalytical and Nuclear Chemistry, 331, 1-9. http://doi.org/10.1007/s10967-022-08254-9
17. Gulgonul, I.; Celik, M.S. (2018) Understanding the flotation separation of Na and K feldspars in the presence of KCl through ion exchange and ion adsorption (Article). Minerals Engineering, 129, 41-46. http://doi.org/10.1016/j.mineng.2018.08.038
18. Schmitz, C.; Burt, D. (1990) The Black Pearl mine, Arizona; Wolframite veins and stockscheider pegmatite related to an albitic stock. Geological Society of America Special Papers, 246, 221-232. http://doi.org/10.1130/SPE246-p221
19. Taylor, J.C. (1985) Technique and Performance of Powder Diffraction in Crystal Structure Studies. Australian Journal of Physics, 38, 519-522. http://doi.org/10.1071/PH850519
20. Ortiz, A.L.; Cumbrera, F.L.; Sánchez-Bajo, F.; Guiberteau, F.; Caruso, R. (2000) Fundamental parameters approach in the Rietveld method: a study of the stability of results versus the accuracy of the instrumental profile. Journal of the European Ceramic Society, 20, 1845-1851. http://doi.org/10.1016/S0955-2219(00)00056-X
21. Dos-Santos, H.N.; Neumann, R.; Ávila, C.A. (2017) Mineral quantification with simultaneous refinement of Ca-Mg carbonates non-stoichiometry by X-Ray diffraction, Rietveld method (Article). Minerals, 7, 164. http://doi.org/10.3390/min7090164
22. Sun, S.; Zhang, X.; Cui, J.; Liang, S. (2020) Identification of the Miller indices of a crystallographic plane: a tutorial and a comprehensive review on fundamental theory, universal methods based on different case studies and matters needing attention. Nanoscale, 12, 16657-16677. http://doi.org/10.1039/d0nr03637d
23. Ali, A.; Chiang, Y.; Santos, R.M. (2022) X-Ray Diffraction Techniques for Mineral Characterization: A Review for Engineers of the Fundamentals, Applications, and Research Directions. Minerals, 12, 205. http://doi.org/10.3390/min12020205
24. Kahle, M.; Kleber, M.; Jahn, R. (2002) Review of XRD-based quantitative analyses of clay minerals in soils: the suitability of mineral intensity factors. Geoderma, 109, 191-205. http://doi.org/10.1016/S0016-7061(02)00175-1
25. Lou, W.; Zhang, D.; Bayless, R.C. (2020) Review of mineral recognition and its future. Applied Geochemistry, 122, 104727. http://doi.org/10.1016/j.apgeochem.2020.104727
26. Li, Z.; Zhang, M.; Yang, Z.; Ding, Cong.; Liu Y.; Huang G. (2023) Application of FTIR and XRD in Coal Structural Analysis of Fault Tectonic. Spectroscopy and Spectral Analysis, 43, 657. http://doi.org/10.3964/j.issn.1000-0593(2023)02-0657-08